Mathematics of a Tetrahedron Chain and the Hamiltonian Cycle Problem

Naoto Morikawa

Abstract. In this article we consider the problem of finding Hamiltonian cycles on a tetrahedral mesh. A Hamiltonian cycle is a closed loop through a tetrahedral mesh that visits each tetrahedron exactly once. Using techniques of a novel discrete differential geometry of n-simplices, we could immediately obtain Hamiltonian cycles on a rhombic dodecahedron-shaped tetrahedral mesh consisting of 24 tetrahedrons. For easier visualization, we firstly consider Hamiltonian cycles on triangular meshes and provide some foundations for the study of the tetrahedral mesh.

1. INTRODUCTION. In this article we consider the problem of finding Hamiltonian cycles on a tetrahedral mesh. A Hamiltonian cycle is a closed loop through a tetrahedral mesh that visits each tetrahedron exactly once. Previously [**1**] and [**2**] study Hamiltonian cycles on a tetrahedral mesh which passes tetrahedrons through a common vertex. In contrast, we study Hamiltonian cycles which passes tetrahedrons through a common face. The reason is that through-face type Hamiltonian cycles give us insights into how a chain of tetrahedrons is folded into a solid shape, where tetrahedrons are connected along hinges that are mutually shared by the edges of adjacent tetrahedrons ([**3**], [**4**]). For example, it is known that a rhombic dodecahedron is obtained by folding a closed chain of 24 isosceles tetrahedrons (Figure 1). This implies there exists a Hamiltonian cycle of tetrahedrons on a rhombic dodecahedron-shaped tetrahedral mesh consisting of 24 tetrahedrons.

Specifically our target is the Hamiltonian cycle problem on the rhombic dodecahedron-shaped tetrahedral mesh (Figure 1). For easier visualization, we also consider Hamiltonian cycles on a triangular mesh (Figure 2) and provide some foundations for the study of the tetrahedral mesh.

Here we give some background knowledge on the topics of tetrahedron chains. Well known from recreational mathematics are rotating rings of tetrahedrons ([**5**], [**6**]). Although they are usually seen as puzzle toys, there also exist their applications to industry. For example, a new retractable structure based on three-symmetric Bricard linkages and rotating rings of tetrahedrons is proposed in [**7**]. As for mechanisms and states of self-stress in the rings, a general analysis is provided by [**8**].

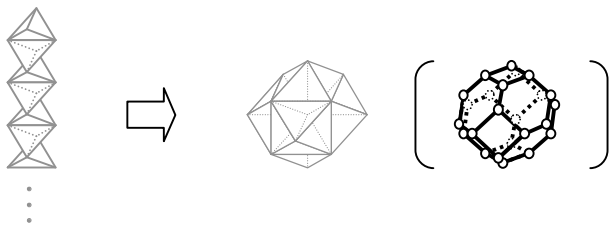

Figure 1. Our problem (A): The Hamiltonian cycle problem on a rhombic dodecahedron-shaped mesh consisting of 24 congruent tetrahedrons. Shown in the brackets is a node and edge-representation of the mesh.

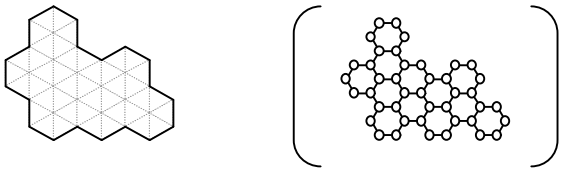

Figure 2. Our problem (B): The Hamiltonian cycle problem on a triangular mesh consisting of 42 congruent isosceles triangles. Shown in the brackets is a node and edge-representation of the mesh.

Also known are chains of interconnected isosceles tetrahedrons which were mentioned in patents [**3**] and [**4**]. The patents describe a transformational folding puzzle assembly formed of a chain of 24 isosceles tetrahedrons, where tetrahedrons are connected along hinges that are mutually shared by the edges of adjacent tetrahedrons. Since the tetrahedrons are space-filling, the chain could be contracted into various solid shapes with no gaps between the tetrahedrons. For example, one could fold the (closed) chain of 24 tetrahedrons into a rhombic dodecahedron as mentioned above.

Lately applications of the latter type of linked tetrahedrons are found in robotics and biotechnology. In the field of self-reconfigurable robotics, [**9**] shows that a chain of right angle isosceles tetrahedrons can be combined with external actuation to form arbitrary shapes. In the filed of protein structure analysis, [**10**] proposes a simple structure encoding method, where fragments of five amino-acids are approximated by a chain of five right angle isosceles tetrahedrons. To translate the conformation of local protein structure into a binary sequence, [**10**] developed a novel discrete differential geometry of tetrahedrons. Unlike previous studies, [**10**] considers connection between space-filling isosceles tetrahedrons and introduces tangent-bundle like structure on a set of tetrahedrons.

This article is an introduction to the mathematical framework behind [**10**], i.e., a discrete differential geometry of n-simplices. Using techniques from the framework, we could obtain Hamiltonian cycles on a triangle/tetrahedral mesh almost instantly (if they exist).

2. HAMILTONIAN CYCLES ON A TRIANGULAR MESH. Let's start with the Hamiltonian cycle problem on the triangular mesh shown in Figure 2. Hamiltonian cycles enter a triangle through a edge and leave the triangle through another edge. In the figures, we use heavy edges to indicate the third edge of a triangle, i.e., the edge which is not used in the Hamiltonian cycle. The boundary of the mesh consists of the heavy edges of 20 triangles because Hamiltonian cycles don't go beyond the boundary.

One notable feature of the triangular mesh is its regularity. In particular, one could associate three-dimensional cubes (3-cubes) over the mesh as shown in Figure 3. We call them a 3-*cube covering* of the mesh. In the figure, each of the three upper faces of a 3-cube is divided into two isosceles triangles by a diagonal segment (heavy line), where the six triangles on the upper faces are projected onto six triangles in the triangular mesh (Figure 3 (a)). We call a triangle on one of the three upper faces of a 3-cube a *slant* triangle. A triangle in the mesh is called a *flat* triangle.

A flat triangle in the mesh corresponds to a slant triangle on a 3-cube over the mesh in such a way that the heavy edge of the slant triangle is projected onto the heavy edge (i.e., the third edge) of the flat triangle. Therefore, the gradient of the slant triangle over a flat triangle indicates the direction of a trajectory on the flat triangle. Note that the correspondence between slant and flat triangles (i.e., a 3-cube covering and the mash,) is not unique. That is, by inverting the up and down of the slant triangles, we would

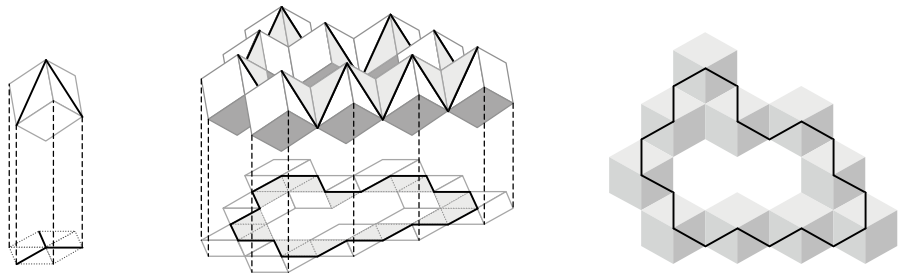

(a) (b) (c)

Figure 3. 3-cubes over a triangular mesh. (a): The correspondence between six slant triangles on the three upper faces of a 3-cube and six flat triangles in a triangular mesh. (b): 3-cubes over the boundary of the triangular mesh of Figure 2. (c): Top view of (b).

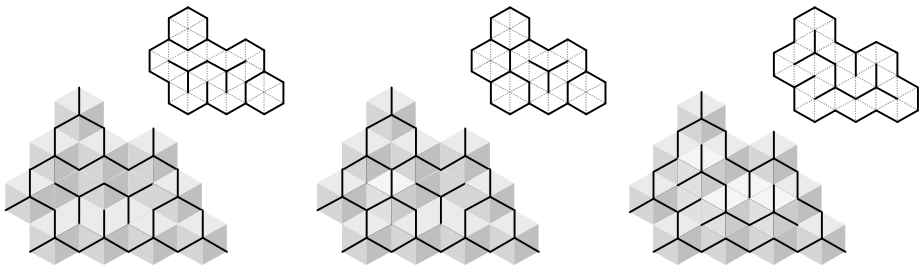

(a) (b) (c)

Figure 4. Top view of 3-cube coverings of the triangular mesh given by Figure 2 and their corresponding closed loop decompositions. (a): The 3-cube covering generated by the triangular cones over the boundary. (b): The 3-cube covering obtained by putting a 3-cube on the covering of (a). (c): The 3-cube covering obtained by putting four 3-cube on the covering of (b).

obtain another 3-cube covering of the mesh. The amount of labor for computation of Hamiltonian cycles, though, does not depend on the kind of 3-cube coverings.

In our case, the boundary of the triangular mesh is covered by ten 3-cubes as shown in Figure 3 (b) and (c). Considering the triangular cones whose top vertices are specified by the 3-cubes, we obtain a 3-cube covering over the whole mesh (Figure 4 (a)). Each cone is obtained by piling up 3-cubes whose upper faces are divided into two isosceles triangles by a diagonal segment (heavy line). By projecting the slant triangles on the cones onto the mesh, we obtain a flow of flat triangles. In the case of Figure 4 (a), the triangular mesh is decomposed into three closed loops of triangles.

A different 3-cube covering over a triangular mesh corresponds to a different flow of triangles on the mesh. For example, by putting a 3-cube on the 3-cube covering of Figure 4 (a), we obtain another 3-cube covering over the mesh. Then, the mesh is decomposed into five closed loops (Figure 4 (b)). Putting four more 3-cubes on the 3-cube covering, we obtain a Hamiltonian cycle of the mesh (Figure 4 (b))).

3. COTANGENT CONES AND A 3-CUBE COVERING. Now let's consider more about the diagonal line segments (heavy lines) on the upper faces of 3-cube coverings. Using the line segments as edges, we could construct another type of 3-cubes over the mesh as shown in Figure 5 (a). We call this type of 3-cube a *cotangent* 3-cube.

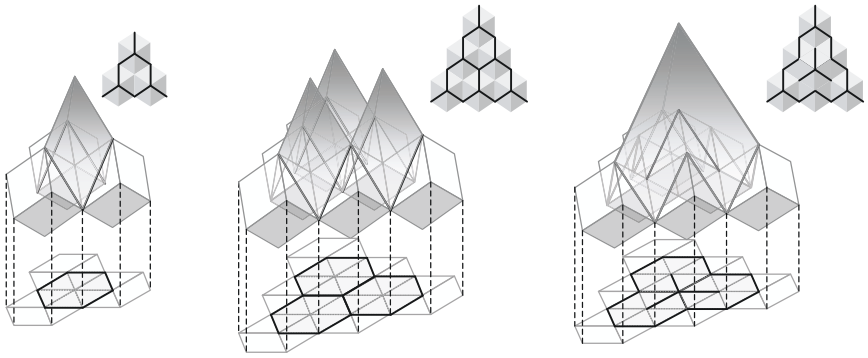

(a) (b) (c)

Figure 5. (a): A 3-cube covering of a hexagon-shaped triangular mesh and the corresponding cotangent 3-cube. (Only the three upper faces of the cotangent cube are shown in the figure.) (b): A 3-cube covering of a triangular mesh and the corresponding three cotangent cones. Three cotangent cones correspond to three closed loops of length six on the mesh, respectively. (c): A 3-cube covering of a triangular mesh and the corresponding cotangent cone. The cotangent cone corresponds to the Hamiltonian cycle on the mesh.

(a) (b)

Figure 6. (a): The corresponding cotangent cones of the 3-cube covering of Figure 4 (a). (b): The corresponding cotangent cones of the 3-cube covering of Figure 4 (c).

A *cotangent* cone is a cone obtained by piling up cotangent 3-cubes. (3-cubes of the original type are called *tangent* cube and cones generated by tangent 3-cubes are called *tangent* cone.) Note that the boundary of the area enclosed by a closed loop of flat triangles on a mesh corresponds to a set of cotangent cones. Roughly speaking, the boundary is given as the projection image of the intersection of the 3-cube covering and the corresponding cotangent cones.

For example, a triangular mesh of Figure 5 (b), which consists of three closed loops of length six, corresponds to three cotangent cones. Each cotangent cone cover the hexagonal area swept by one of the closed loops. Putting a 3-cube on the 3-cube covering of the mesh, we obtain a Hamilton cycle of the mesh (Figure 5 (c)). The boundary of the mesh corresponds to the intersection of a cotangent cone and the 3-cube covering as shown in the figure. In particular, all the slant triangles over the mesh are contained in the cotangent cone.

Figure 6 (a) and (b) shows the corresponding cotangent cones of the 3-cube coverings of Figure 4 (a) and (c) respectively. In the case of Figure 6 (a), the longer loop is covered by a set of three cotangent cones and each of the two shorter loops are covered

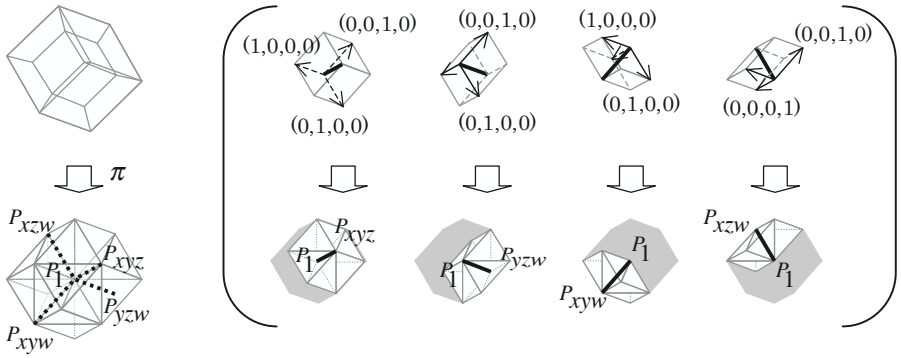

Figure 7. The correspondence between a 4-cube (represented by the Schlegel diagram) and 24 tetrahedrons in a tetrahedral mesh, where $P_1 = \pi((0,0,0,0))$, $P_{xyz} = \pi((1,1,1,0))$, $P_{xzw} = \pi((1,0,1,1)$, $P_{xyw} = \pi((1,1,0,1)$, and $P_{yzw} = \pi((0,1,1,1)$. Shown in the brackets are the four upper facets of the 4-cube and their projection images on $\mathbf{R}^3$. The diagonal line segment of each facet is indicated by heavy line.

by a cotangent cone. In the case of Figure 6 (b), the Hamiltonian cycle corresponds to a set of three cotangent cones.

4. HAMILTONIAN CYCLES ON A TETRAHEDRAL MESH. Having provided foundations for the study of tetrahedral meshes, we would now consider the Hamiltonian cycle problem on the dodecahedron-shaped mesh of Figure 1.

In the case of tetrahedral meshes, we associate four-dimensional cubes (4-cubes) over a mesh as shown in Figure 7. The projection π from four-dimensional Euclidean space $\mathbf{R}^4$ onto three-dimensional Euclidean space $\mathbf{R}^3$ is given by the following equations: $\pi((l,m,n,k)) = (a,b,c)$, where

$$a := (l-n)/\sqrt{2},$$
$$b := (m-k)/\sqrt{2},$$
$$c := (l-m+n-k)/2.$$

Roughly speaking, π is a projection of $\mathbf{R}^4$ onto the hyperplane defined by $l+m+n+k=0$. In particular, $\pi((l+1,m+1,n+1,k+1)) = \pi(l,m,n,k)$. We then consider the image of the four upper facets (i.e., face of dimension three) of 4-cubes on the hyperplane.

Each upper facet of a 4-cube is divided into six tetrahedrons along the diagonal line segment (heavy line) of the facet as shown in the brackets of Figure 7. We call the six tetrahedrons a *slant* tetrahedron. Slant tetrahedrons are projected onto tetrahedrons in the tetrahedral mesh, which are called *flat* tetrahedrons. In particular, each flat tetrahedron consists of four short edges and two long edges, where the ratio of the length is $\sqrt{3}/2$. The tetrahedron chain shown in Figure 1 is obtained by connecting successive tetrahedrons via a long edge. The chain has a rotational freedom around the long edges and is folded into a wide variety of shapes.

As is the case with triangular meshes, we only permit trajectories along the diagonal line segments (i.e., one of four short edges of a flat tetrahedron) on a tetrahedral mesh. A trajectory of tetrahedrons enters a tetrahedron through a face and leave the tetrahe-

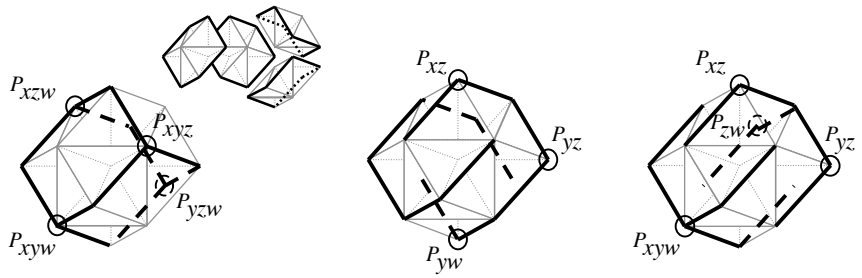

(a) (b) (c)

Figure 8. Closed loops on a rhombic dodecahedron-shaped mesh of 24 tetrahedrons. (In the figures, $P_{xz} = \pi((1,0,1,0)$, $P_{yz} = \pi((0,1,1,0)$, $P_{yw} = \pi((0,1,0,1)$, and so on.) (a): Four closed loops induced by the 4-cube covering generated by the cones over the boundary whose top vertices are $(1,1,1,0)$, $(1,0,1,1)$, $(1,1,0,1)$ and $(0,1,1,1)$. (b): The Hamiltonian cycle induced by the 4-cube covering of three peaks $(1,0,1,0)$, $(0,1,1,0)$ and $(0,1,0,1)$. (c): The Hamiltonian cycle induced by the 4-cube covering of four peaks $(1,1,0,1)$, $(1,0,1,0)$, $(0,1,1,0)$, and $(0,0,1,1)$.

dron through one of the two faces which share a short edge with the entrance face. In particular, any trajectory on a tetrahedral mesh could be obtained by folding the tetrahedral chain (of adequate length) given in Figure 1. Note that all but one short edges of a tetrahedron are contained in the entrance face or the exit face of the tetrahedron. That is, the fourth short edge of a tetrahedron on a trajectory determines the direction of the trajectory at the tetrahedron. In the figures, we use heavy line to indicate the fourth short edge of a tetrahedron.

5. HAMILTONIAN CYCLES ON A RHOMBIC DODECAHEDRON-SHAPED MESH. Finally let's consider the Hamiltonian cycle problem on the rhombic dodecahedron-shaped tetrahedral mesh (Figure 1). In this case, the boundary is covered by four 4-cubes, whose top vertices are $(1,1,1,0)$, $(1,0,1,1)$, $(1,1,0,1)$ and $(0,1,1,1)$. Considering the four-dimensional cones whose top vertices are specified by the four 4-cubes, we obtain a 4-cube covering over the whole mesh. By projecting the slant tetrahedrons on the 4-cube covering onto the tetrahedral mesh, we obtain a flow of flat tetrahedrons (Figure 8(a)). The mesh is then decomposed into four closed loops of six tetrahedrons as shown in the figure. The four closed loops correspond to a cotangent cone of top vertex $(0,0,0,0)$. (Unlike the case of triangular meshes, we couldn't distinguish the four loops from each other using a set of cotangent cones. Note that, since the "cotangent" lattice is generated by four vectors $(1,1,1,0)$, $(1,1,0,1)$, $(1,0,1,1)$, and $(0,1,1,1)$, it is rougher than the "standard" lattice which is generated by four vectors $(1,0,0,0)$, $(0,1,0,0)$, $(0,0,1,0)$, and (0,0,0,1).)

Putting 4-cubes on the 4-cube covering, we obtain other 4-cube coverings. Unlike the case of triangular meshes, some of the slant tetrahedrons over a tetrahedral mesh are not contained in any of the corresponding cotangent cones. However, a slant tetrahedron would not be projected onto a tetrahedral mesh if it doesn't intersect with any of the corresponding cotangent cones. In our case, it is enough to consider the 4-cubes contained in the tangent cone with top vertex $(0,0,0,0)$ since the corresponding set of cotangent cones consists of a cone with vertex $(0,0,0,0)$. (That is, we would obtain all the 4-cube coverings over the mesh by removing 4-cubes from the tangent cone with top vertex $(0,0,0,0)$. See Appendix A for a detailed description of the process.)

By considering all the 4-cube coverings over the rhombic dodecahedron-shaped

mesh, we obtain two Hamiltonian cycles on the mesh. Figure 7 (b) shows the 4-cube covering of the mesh specified by three 4-cones, whose top vertices are $(1,0,1,0)$, $(0,1,1,0)$ and $(0,1,0,1)$. The covering gives a Hamiltonian cycle of the mesh. Note that vertices $(1,0,1,0)$, $(0,1,1,0)$, $(0,1,0,1)$ are not contained in the corresponding cotangent cone of top vertex $(0,0,0,0)$. Figure 7 (c) shows the 4-cube covering of the mesh specified by four 4-cones, whose top vertices are $(1,1,0,1)$, $(1,0,1,0)$, $(0,1,1,0)$, and $(0,0,1,1)$. The covering gives the other Hamiltonian cycle of the mesh.

6. CONCLUSION. We have solved the Hamiltonian cycle problem on a tetrahedral mesh by piling up 4-cubes diagonally on the mesh. To provide foundation of the mathematical framework we use, we started this article with the Hamiltonian cycle problem on triangular meshes.

In the case of triangular meshes, we could describe a closed trajectory algebraically with a set of tangent cones and a set of cotangent cones. Particularly the slant triangles on a trajectory are contained in the corresponding set of cotangent cones. On the other hand, there exists no such clear correspondence between a trajectory and the corresponding tangent/cotangent cones in the case of tetrahedral meshes. The slant tetrahedrons on a trajectory, however, intersect with one of the corresponding set of cotangent cones. Therefore, the process of piling up 4-cubes will terminate in a finite number of steps. For the detailed computation process, see Appendix A.

Software program (tetrahedron flow viewer) *HeteroNumberViewer* is available from [**11**].

REFERENCES

1. W.F. Mitchell, Hamiltonian paths through two- and three-dimensional grids, *J. Res. NIST* **110** (2005) 127-136.
2. H. Liu, L. Zhang: Existence and construction of Hamiltonian paths and cycles on conforming tetrahedral meshes. *Int. J. Comput. Math.* **88(6)** (2011) 1137-1143.
3. A. P. Coppa, (1976) Three-dimensional folded chain structures. US Patent No.4142321 A.
4. R. E. Schaedel, (1998) Folding puzzle/transformational toy with 24 linked tetrahedral elements. US Patent No.6264199 B1.
5. R.M. Stalker, (1933) Advertising medium or toy. US Patent No.1997022 A.
6. W.W.Rouse Ball *Mathematical Recreations and Essays*, 11th edition. Revised and extended by H.S.M. Coxeter, London: Macmillan and Co., Ltd. 1939.
7. Y. Luo, Y. Yu, J. Liu , A retractable structure based on Bricard linkages and rotating rings of tetrahedra, *International Journal of Solids and Structures* **45** (2008) 620-630.
8. P.W. Fowler, S.D.Guest, A symmetry analysis of mechanisms in rotating rings of tetrahedra. *Proc. R. Soc. A* **461(2058)**, (2005) 1829-1846.
9. P. J. White, C. E. Thorne, and M. Yim, Right Angle Tetrahedron Chain Externally-actuated Testbed (RATChET): A Shape-Changing System, *Proceedings of IDETC/CIE*, San Diego, CA, USA. **7** (2009) 807-817.
10. N.Morikawa, Discrete Differential Geometry of n-Simplices and Protein Structure Analysis, *Applied Mathematics* **5** (2014) 2458-2463.
11. N.Morikawa, HeteroNumberViewer. http://www.genocript.com/hetero_number_viewer.html

NAOTO MORIKAWA received his M.S. in mathematics from the University of Tokyo. He is developing software tools for protein structure analysis and others. His is currently interested in the algebra of closed loops of triangles/tetrahedrons and its application to protein complex (i.e., a group of two or more associated proteins) description.

Genocript, 27-22-1015, Sagami-ga-oka 1-chome, Zama-shi, Kanagawa 228-0001 Japan
nmorika@genocript.com

A. COMPUTATION OF FLOWS ON THE RHOMBIC DODECAHEDRON-SHAPED TETRAHEDRAL MESH. We could compute all the 4-cube coverings of the rhombic dodecahedron-shaped tetrahedral mesh by removing 4-cubes from the tangent cone with top vertex $(0,0,0,0)$. In the following, $Cone\{v_1, v_2, ..., v_k\}$ $(v_i \in R^4)$ denotes the 4-cube covering with peaks $v_1, v_2, ..., v_k$. (In particular, $Cone\{(x,y,z,w)\}$ is the tangent cone with top vertex (x,y,z,w).)

[Step0] Initial 4-cube covering. We start with $Cone\{(0,0,0,0)\}$. Shown below is the flow induced on the rhombic dodecahedron-shaped tetrahedral mesh by 4-cube covering $Cone\{(0,0,0,0)\}$, where $P_{x^l y^m z^n w^k} = \pi((l,m,n,k)) = ((l-n)/\sqrt{2}, (m-k)/\sqrt{2}, (l-m+n-k)/2) \in R^3$. Recall that diagonal line segments (heavy line) indicate the direction of a trajectory at the tetrahedron.

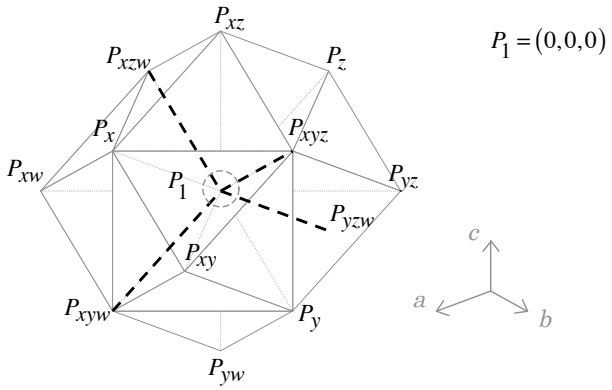

Figure 9. Step0: The flow induced by $Cone\{(0,0,0,0)\}$

[Step1] Remove a 4-cube at $(0,0,0,0)$. By removing a 4-cube at $(0,0,0,0)$ from 4-cube covering $Cone\{(0,0,0,0)\}$, we obtain 4-cube covering $Cone\{(1,0,0,0), (0,1,0,0), (0,0,1,0), (0,0,0,1)\}$.

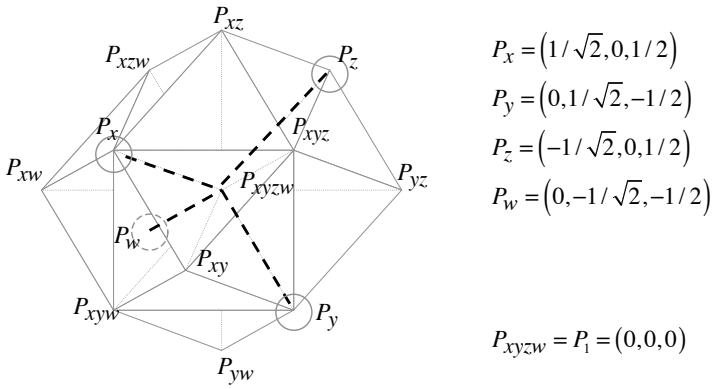

Figure 10. Step1: The flow induced by $Cone\{(1,0,0,0), (0,1,0,0), (0,0,1,0), (0,0,0,1)\}$

[Step2] Remove a 4-cube at $(1,0,0,0)$. By removing a 4-cube at $(1,0,0,0)$ from $Cone\{(1,0,0,0),(0,1,0,0),(0,0,1,0),(0,0,0,1)\}$, we obtain $Cone\{(2,0,0,0),(0,1,0,0),(0,0,1,0),(0,0,0,1)\}$.

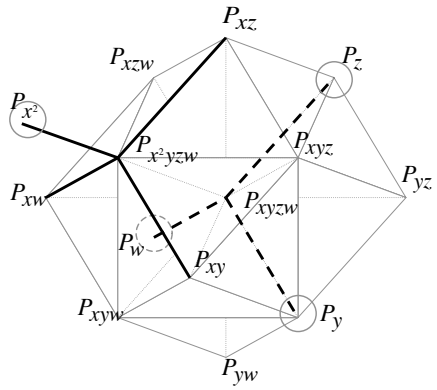

$P_{x^2} = \left(\sqrt{2},0,1\right)$
$P_y = \left(0,1/\sqrt{2},-1/2\right)$
$P_z = \left(-1/\sqrt{2},0,1/2\right)$
$P_w = \left(0,-1/\sqrt{2},-1/2\right)$

$P_{x^2yzw} = P_x = \left(1/\sqrt{2},0,1/2\right)$

Figure 11. Step2: The flow induced by $Cone\{(2,0,0,0),(0,1,0,0),(0,0,1,0),(0,0,0,1)\}$

[Step3] Remove a 4-cube at $(0,1,0,0)$. By removing a 4-cube at $(0,1,0,0)$ from $Cone\{(2,0,0,0),(0,1,0,0),(0,0,1,0),(0,0,0,1)\}$, we obtain $Cone\{(1,1,0,0),(2,0,0,0),(0,2,0,0),(0,0,1,0),(0,0,0,1)\}$.

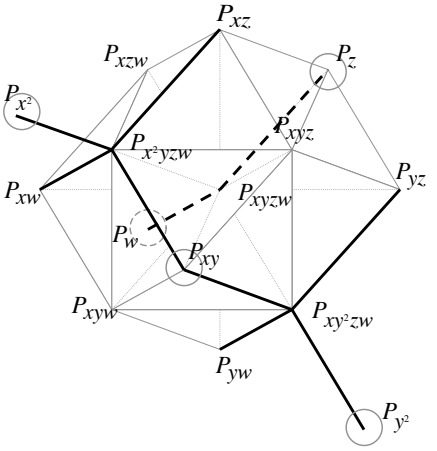

$P_{xy} = \left(1/\sqrt{2},1/\sqrt{2},0\right)$
$P_{x^2} = \left(\sqrt{2},0,1\right)$
$P_{y^2} = \left(0,\sqrt{2},-1\right)$
$P_z = \left(-1/\sqrt{2},0,1/2\right)$
$P_w = \left(0,-1/\sqrt{2},-1/2\right)$

$P_{xy^2zw} = P_y = \left(0,1/\sqrt{2},-1/2\right)$

Figure 12. Step3: The flow induced by $Cone\{(1,1,0,0),(2,0,0,0),(0,2,0,0),(0,0,1,0),(0,0,0,1)\}$

[Step4] Remove a 4-cube at $(0,0,1,0)$. By removing a 4-cube at $(0,0,1,0)$ from $Cone\{(1,1,0,0),(2,0,0,0),(0,2,0,0),(0,0,1,0),(0,0,0,1)\}$, we obtain the flow shown below. There is a closed loop of length six. Note that peaks $(2,0,0,0$, $(0,2,0,0)$, and $(0,0,2,0)$ have no influence on the flow.

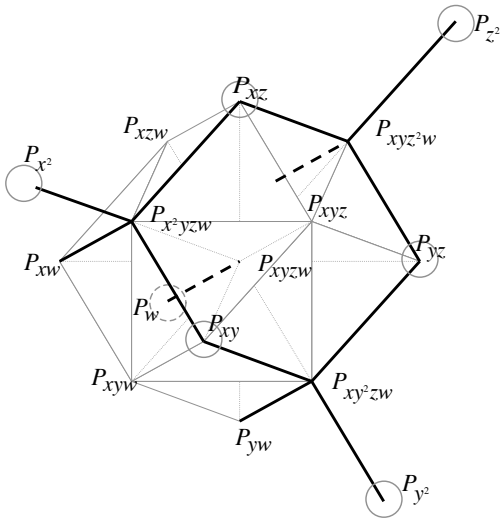

$$P_{xy}=\left(1/\sqrt{2},1/\sqrt{2},0\right)$$
$$P_{xz}=(0,0,1)$$
$$P_{yz}=\left(-1/\sqrt{2},1/\sqrt{2},0\right)$$
$$P_{w}=\left(0,-1/\sqrt{2},-1/2\right)$$
$$P_{xyz^2w}=P_z=\left(-1/\sqrt{2},0,-1/2\right)$$

Figure 13. Step4: The flow induced by $Cone\{(1,1,0,0),(1,0,1,0),(0,1,1,0),(2,0,0,0),(0,2,0,0),$ $(0,0,2,0),(0,0,0,1)\}$

[Step5] Remove a 4-cube at $(0,0,0,1)$. By removing a 4-cube at $(0,0,0,1)$ from $Cone\{(1,1,0,0),(1,0,1,0),(0,1,1,0),(2,0,0,0),(0,2,0,0),\ (0,0,2,0),$ $(0,0,0,1)\}$, we obtain the flow shown below. We also remove peaks $(2,0,0,0$, $(0,2,0,0)$, $(0,0,2,0)$, and $(0,0,0,2)$ from the 4-cube covering because they have no influence on the flow. There are four closed loops of length six.

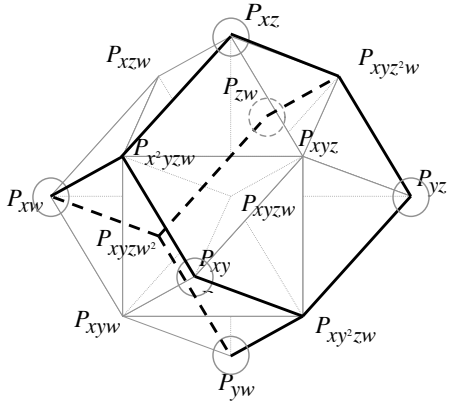

$$P_{xy}=\left(1/\sqrt{2},1/\sqrt{2},0\right)$$
$$P_{xz}=(0,0,1)$$
$$P_{xw}=\left(1/\sqrt{2},-1/\sqrt{2},0\right)$$
$$P_{yz}=\left(-1/\sqrt{2},1/\sqrt{2},0\right)$$
$$P_{yw}=(0,0,-1)$$
$$P_{zw}=\left(-1/\sqrt{2},-1/\sqrt{2},0\right)$$
$$P_{xyzw^2}=P_w=\left(0,-1/\sqrt{2},-1/2\right)$$

Figure 14. Step5: The flow induced by $Cone\{(1,1,0,0),(1,0,1,0),(1,0,0,1),(0,1,1,0),\ (0,1,0,1),$ $(0,0,1,1)\}$

[Step6] Remove a 4-cube at $(1,1,0,0)$. By removing a 4-cube at $(1,1,0,0)$ from $Cone\{(1,1,0,0),(1,0,1,0),(1,0,0,1),(0,1,1,0),\ (0,1,0,1),\ (0,0,1,1)\}$, we obtain the flow shown below. There are two closed loops of length six and one closed loop of length 12.

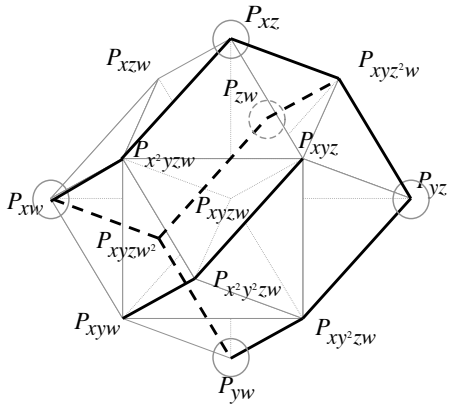

$$P_{xz}=(0,0,1)$$
$$P_{xw}=\left(1/\sqrt{2},-1/\sqrt{2},0\right)$$
$$P_{yz}=\left(-1/\sqrt{2},1/\sqrt{2},0\right)$$
$$P_{yw}=(0,0,-1)$$
$$P_{zw}=\left(-1/\sqrt{2},-1/\sqrt{2},0\right)$$
$$P_{x^2y^2zw}=P_{xy}=\left(1/\sqrt{2},1/\sqrt{2},0\right)$$

Figure 15. Step6: The flow induced by $Cone\{(1,0,1,0),(1,0,0,1),(0,1,1,0),(0,1,0,1),(0,0,1,1)\}$

[Step7] Remove a 4-cube at $(1,0,0,1)$. By removing a 4-cube at $(1,0,0,1)$ from $Cone\{(1,0,1,0),(1,0,0,1),(0,1,1,0),(0,1,0,1),(0,0,1,1)\}$, we obtain the flow shown below. There are one closed loop of length six and one closed loop of length 18.

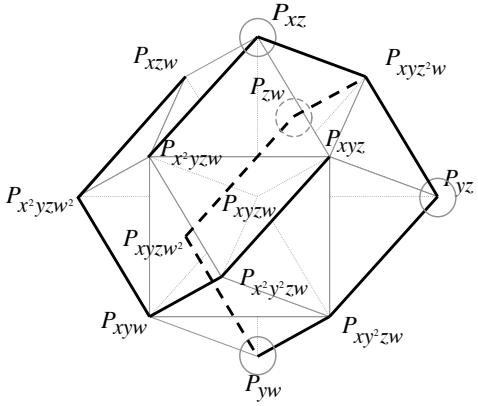

$$P_{xz}=(0,0,1)$$
$$P_{yz}=\left(-1/\sqrt{2},1/\sqrt{2},0\right)$$
$$P_{yw}=(0,0,-1)$$
$$P_{zw}=\left(-1/\sqrt{2},-1/\sqrt{2},0\right)$$
$$P_{x^2yzw^2}=P_{xw}=\left(1/\sqrt{2},-1/\sqrt{2},0\right)$$

Figure 16. Step7: The flow induced by $Cone\{(1,0,1,0),(0,1,1,0),(0,1,0,1),(0,0,1,1)\}$

[Step8a] Remove a 4-cube at $(0,0,1,1)$. By removing a 4-cube at $(0,0,1,1)$ from $Cone\{(1,0,1,0),(0,1,1,0),(0,1,0,1),(0,0,1,1)\}$, we obtain the flow shown below. There is a closed loops of length 24, i.e., we obtain a Hamiltonian cycle of the mesh.

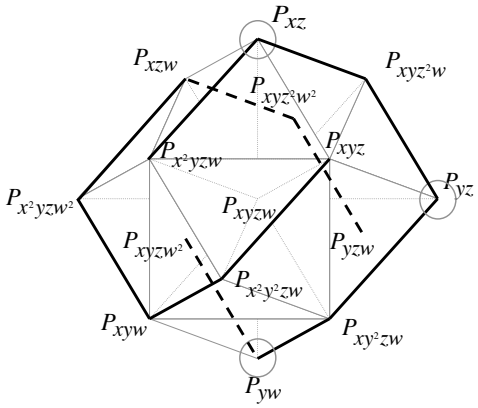

$$P_{xz}=(0,0,1)$$
$$P_{yz}=\left(-1/\sqrt{2},1/\sqrt{2},0\right)$$
$$P_{yw}=(0,0,-1)$$

$$P_{xyz^2w^2}=P_{zw}=\left(-1/\sqrt{2},-1/\sqrt{2},0\right)$$

Figure 17. Step8a: The flow induced by $Cone\{(1,0,1,0),(0,1,1,0),(0,1,0,1)\}$

[Step8b] Remove a 4-cube at $(0,1,0,1)$. By removing a 4-cube at $(0,1,0,1)$ from $Cone\{(1,0,1,0),(0,1,1,0),(0,1,0,1),(0,0,1,1)\}$, we obtain the flow shown below. We obtain another Hamiltonian cycle of the mesh. In the computation process, we see some closed loops of tetrahedrons. As for the loops of length 24, there exists 17 kinds of closed loops of tetrahedrons. That is, we would obtain 17 kinds of solid shapes by folding the (closed) tetrahedron chain of length 24 given in Figure 1. Two of them are obtained in this article. See Appendix B for the distribution of length of closed trajectories of tetrahedrons and others.

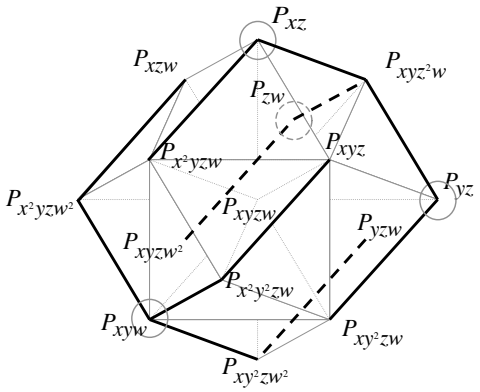

$$P_{xz}=(0,0,1)$$
$$P_{yz}=\left(-1/\sqrt{2},1/\sqrt{2},0\right)$$
$$P_{zw}=\left(-1/\sqrt{2},-1/\sqrt{2},0\right)$$
$$P_{xyw}=\left(1/\sqrt{2},0,-1/2\right)$$

$$P_{xy^2zw^2}=P_{yw}=(0,0,-1)$$

Figure 18. Step8b: The flow induced by $Cone\{(1,0,1,0),(0,1,1,0),(0,0,1,1),(1,1,0,1)\}$

B. THE DISTRIBUTION OF LENGTH OF CLOSED TRAJECTORIES. Shown below is the distribution of length of closed trajectories of triangles, tetrahedrons, and other n-simplices (As for meshes of n-simplices, see [**10**]). In the table, closed trajectories with the same folding pattern are identified. Roughly speaking, two closed trajectories are identified if and only if they coincide with each other by rotational shift, inversion, or reversion.

Table 1. The distribution of length of closed trajectories

Length	*Triangular mesh*	*Tetrahedral mesh*	*4-simplicial mesh*	*5-simplicial mesh*	*6-simplicial mesh*
2	0	0	0	0	0
4	0	0	0	0	0
6	1	1	1	1	1
8	0	0	0	0	0
10	1	0	0	0	0
12	0	3	2	2	2
14	2	0	1	0	0
16	0	0	1	2	1
18	5	6	3	3	4
20	0	0	4	3	3
22	11	0	3	3	1
24	0	17	4	6	9
26	27	0	5	6	3
28	0	0	13	10	10
30	78	42	10	5	10
32	0	0	10	17	11
34	234	0	12	6	7
36	0	118	41	28	30
38	778	0	29	25	15
40	0	0	24	30	30
42	2831	391	49	48	33
44	0	0	122	42	59
46	11122	0	91	70	35
48	0	1301	109	100	100
total	15090	1879	534	407	364